Cyclic failure characteristics of silty sands with the presence of initial shear stress

Xiao Wei[1], Zhongxuan Yang[1], and Jun Yang[3]*

[1] Zhejiang University, Hangzhou, Zhejiang, China
[2] University of Hong Kong, Hong Kong, China
* junyang@hku.hk

Abstract. The liquefaction of silty sands remains an outstanding issue since it triggers catastrophic hazards in recent earthquake events. The cyclic failure pattern is one of the fundamental aspects of liquefaction analysis. However, due to various influencing factors, such as packing density, confining pressure, initial shear stress, cyclic loading amplitude, etc, the failure patterns are less well understood and the underlying mechanism remains unclear. This study presents a series of laboratory testing results to identify the cyclic failure patterns of silty sands considering different soil states, fines contents, initial static shear stress, etc. The key finding is that the failure patterns are related to the states of soils and the cyclic loading characteristics, i.e., the combination of initial shear stress and cyclic loading amplitude. Limitations of the existing prediction methods are discussed, and future work is also suggested.

Keywords: Liquefaction, Cyclic Loading, Failure Patterns, Silty Sand, Initial Shear.

1 Introduction

Soil liquefaction remains an unsolved problem in practice and research even after decades of investigations since the 1964 Niigata earthquake. Ishihara [1] suggested a flow chart for liquefaction assessment considering level and sloping ground conditions, under which different stress states on the soil element can be induced (Fig. 1). The initial stress state of an element beneath level ground is presented in Fig. 1a, where the initial static shear stress (τ_s) on the horizontal surface of the element is zero. The stress state of an element beneath sloping ground is presented in Fig. 1b. The presence of τ_s on the horizontal surface of the element is an important feature that can alter the reversal conditions of the seismic stress cycles (Fig. 1c to e).

Ishihara's procedure [1] suggested that identifying failure patterns of sand is one of the important steps that different failure patterns of the soil require different methods of analysis. Based on the experimental study using clean sands, several types of failure patterns have been identified, including flow-type failures, cyclic mobility, and plastic strain accumulation (e.g., [2, 3]) depending on the packing density of the sands and the reversal conditions of the cyclic stress [3, 4]. Some researchers also suggested

correlations between the monotonic and the cyclic soil responses [4, 5]. It should be noted that most of the previous investigations focused on the liquefaction resistance of sands (e.g., [6, 7]), but there have been relatively fewer investigations on the failure patterns of sands, and thus, there is no reliable framework to predict the cyclic failure patterns. Moreover, most of these studies focusing on the cyclic failure patterns of sands are based on limited testing conditions.

In recent earthquake events [8, 9], liquefaction of silty sands has induced extensive damages and catastrophic hazards. This is partly because current liquefaction assessment methods are mainly based on clean sands, while the liquefaction characteristics of silty sands remain less well understood [10]. This study presents a systematic experimental program together with a detailed analysis of the failure patterns of silty sands under a variety of initial states of soil and loading conditions. Several important factors affecting the failure patterns of silty sands are identified and discussed.

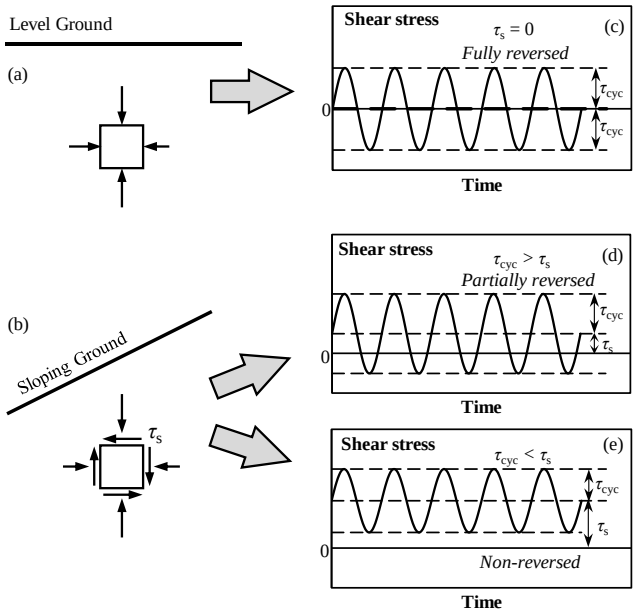

Fig. 1. Initial shear stress induced by ground conditions, and reversal conditions of stress cycles

2 Experimental Program

2.1 Materials

Toyoura sand (TS) is a uniform silica sand that consists of mainly sub-angular particles. Non-plastic crushed silica fines were added into Toyoura sand at different fines contents (FC), forming silty sands with well-controlled properties. The silty sands are denoted by TSS with a number indicating the fines content (e.g., TSS10 is the mixture

with FC = 10%). The particle size distribution curves of the test materials are presented in Fig. 2 and the basic properties of these materials are summarized in Table 1.

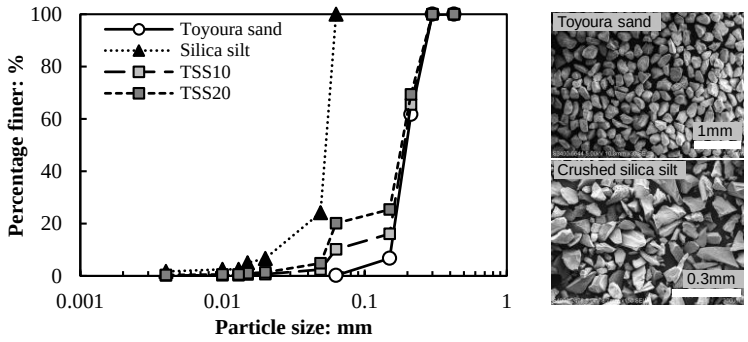

Fig. 2. Particle size distribution curves and SEM images of the tested materials

Table 1. Basic properties of the tested materials

Material	G_s	D_{50}	C_u	e_{max}	e_{min}
Toyoura sand	2.64	0.199	1.37	0.977	0.605
Crushed silica silt	2.65	0.054	2.17	-	-

2.2 Testing procedures

Specimens (diameter = 71.1mm, height = 142.2mm) were reconstituted by the moist tamping method with the under-compaction technique[11]. After the percolation of CO_2 and de-aired water, the specimens were saturated by increasing the back pressure to at least 300kPa or achieving a *B* value of at least 0.95.

In triaxial tests, the stress state on the maximum shear stress plane (the inclined plane with an angle of 45 °to the horizontal plane) is used to simulate the stress state on the horizontal plane of a soil element that is subjected to seismic loading [12]. For a stress state without initial static shear stress, the specimen was consolidated isotropically. For a stress state with non-zero initial static shear stress, the specimen was anisotropically consolidated by increasing the axial and the radial stresses in small increments, maintaining a constant stress ratio until the desired stress condition was reached. The initial static shear stress ratio, α, is defined by the following equation

$$\alpha = \frac{q_s}{2\sigma'_{nc}} = \frac{\sigma'_{1c} - \sigma'_{3c}}{\sigma'_{1c} + \sigma'_{3c}} \tag{1}$$

where q_s is the initial static deviatoric shear stress; $\sigma'_{nc} = (\sigma'_{1c} + \sigma'_{3c})/2$, is the effective normal stress on the maximum shear stress plane of the specimen, after consolidation; σ'_{1c} and σ'_{3c} are the axial and the radial effective stress after consolidation. After consolidation, deviatoric stress cyclces with an amplitude of q_{cyc} were applied to the specimen under undrained conditions. The amplitude of the cyclic loading is characterized by the cyclic shear stress ratio, *CSR*, defined as follows.

$$CSR = \frac{q_{cyc}}{2\sigma'_{nc}} \tag{2}$$

3 Failure characteristics

3.1 Typical failure patterns

The typical failure patterns can be categorized into three general types, namely flow-type failure, cyclic mobility, and strain accumulation. The packing density of the specimen is one of the major factors affecting the failure patterns. For specimens at a relatively loose state, flow-type failure may take place. Fig. 3 presents a typical flow-type failure, in which the specimen has a post-consolidation void ratio (e_c) of 0.906. This type of failure is characterized by a sudden and rapid development of axial strain (ε_a) without a significant pre-failure strain development, after a certain level of excess pore water pressure (Δu) development. The three plots in Fig. 3 are the stress-strain relationship (q-ε_a), stress path in the q-p' plane, and excess pore water pressure generation with the number of stress cycles (N). Fig. 4 presents one more example of flow-type failure for a loose specimen (e_c = 0.907), but with α = 0.4. A major difference between the failure characteristics of the two specimens is that the direction of flow. For the specimen with α = 0, the specimen failed in the triaxial extension side, but the specimen with α = 0.4 failed in the triaxial compression side. This is due to biased cyclic stress caused by the presence of initial shear stress.

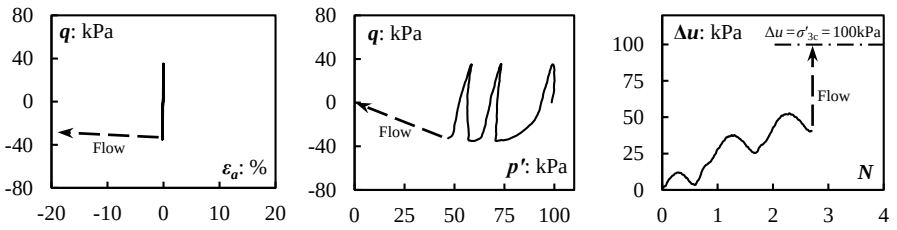

Fig. 3. Flow-type failure for TSS10, e_c = 0.906, α = 0, σ'_{nc} = 100kPa, CSR = 0.175

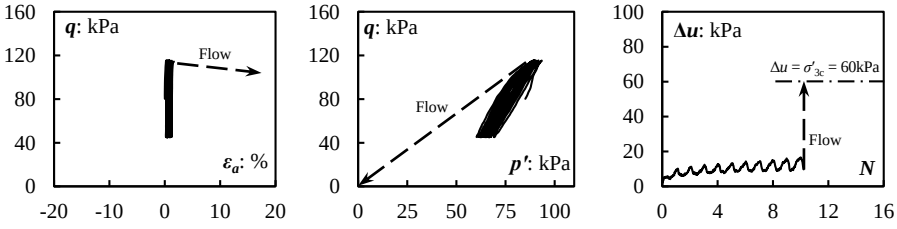

Fig. 4. Flow-type failure for TSS10, e_c = 0.907, α = 0.4, σ'_{nc} = 100kPa, CSR = 0.175

For relatively dense specimens, there are two types of failure patterns depending on the reversal conditions of the cyclic stress. Fig. 5 presents a specimen loaded by

reversed cyclic stress, exhibiting a typical failure pattern known as cyclic mobility. The excess pore water pressure increases while the effective stress decreases cyclically until a state called "initial liquefaction" is reached, where the effective stress transiently equals zero for the first time. The specimen undergoes two transient liquefaction states during each subsequent stress cycle when the deviatoric stress reverses its direction, and large deformation takes place when the state of the specimen is reaching the transient liquefied state. Then, the stiffness and the strength of the specimen recovered due to dilation in the following loading process. Fig. 6 presents an example of plastic strain accumulation, the other type of failure pattern for dense specimens, which occurs if the cyclic stress does not reverse its direction. The major characteristic of this type of failure is the continuous accumulation of irrecoverable strain (i.e., plastic strain) in each stress cycle. The effective stress may never achieve zero even if the deviatoric stress arrived at zero in each cycle. One more characteristic of the specimen is the generation of negative excess pore water pressure due to dilation of the specimen.

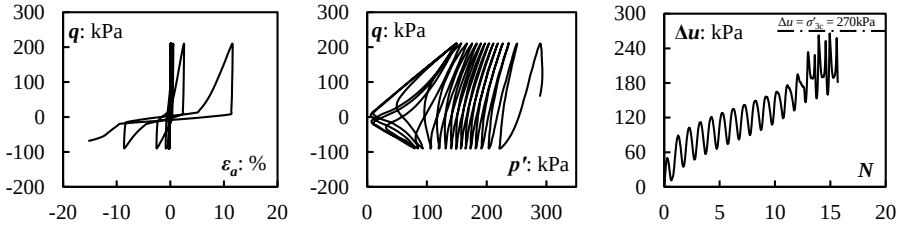

Fig. 5. Cyclic mobility for TSS10, e_c = 0.795, α = 0.1, σ'_{nc} = 300kPa, *CSR* = 0.25

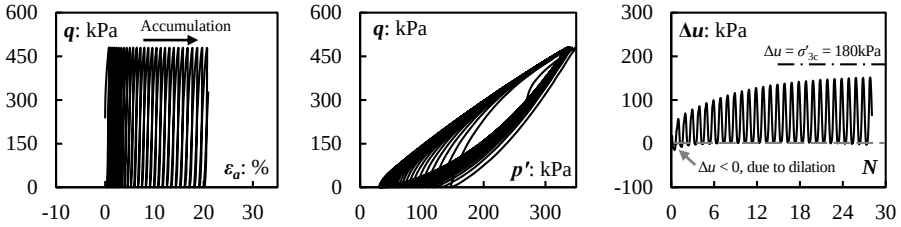

Fig. 6. Plastic strain accumulation for TSS10, e_c = 0.793, α = 0.4, σ'_{nc} = 300kPa, *CSR* = 0.4

3.2 Factors affecting failure patterns

It has been shown that the failure patterns can be affected by the packing density and the reversal condition of the cyclic loading. However, there are other factors that could alter the failure pattern of the specimens even when the packing density is the same and the reversal condition does not change.

Fig. 7 presents an example that confining pressure can change the failure patterns. When the effective stress is 100kPa, the TSS20 specimen with an initial void ratio of 0.796 exhibits plastic strain accumulation under the condition of *CSR* = α = 0.4 (Fig. 7a). However, when the effective stress is 300kPa, the TSS20 specimen with the same

initial void ratio (e_c = 0.796) exhibit flow-type failure for α = 0.4, while *CSR* = 0.25 (Fig. 7b). In addition, Fig. 8 presents an example that the failure pattern is affected by the loading condition. The two specimens with nearly the same void ratio (e_c = 0.847 and 0.849) were loaded by fully reversed stress cycles, i.e., α = 0. For *CSR* = 0.15, cyclic mobility is observed as shown in Fig. 8a, while for *CSR* = 0.2, flow-type failure takes place as shown in Fig. 8b. The results from the two specimens indicate that the cyclic failure pattern can be affected by a small change in the amplitude of cyclic stress.

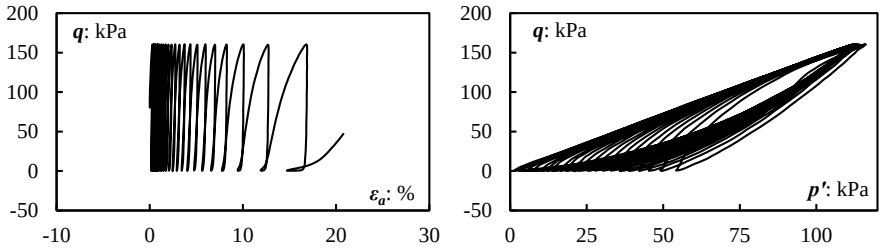

(a) Plastic strain accumulation: σ'_{nc} = 100kPa, *CSR* = 0.4

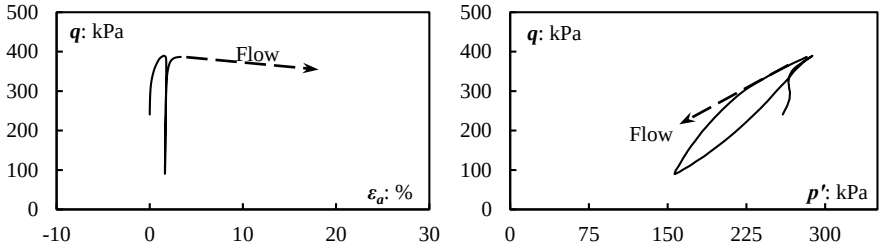

(b) Flow-type failure σ'_{nc} = 300kPa, *CSR* = 0.25

Fig. 7. Effect of confining stress on failure patterns (TSS20, e_c = 0.796, α = 0.4)

4 Discussions

Mohamad and Dobry [4], as well as Chiaro et al. [5], have proposed empirical charts to predict the cyclic failure patterns of sands, by considering the reversal condition of the cyclic stress (i.e., combining initial static shear stress and the cyclic stress amplitude) and the monotonic shearing behavior of the sand. However, these proposed charts are based on limited initial states. Fig. 9 presents a summary of the failure patterns that are observed for the TSS10 and TSS20, regarding the effects of void ratio and confining pressure. It is clear that the failure patterns are dependent on the initial states of sands, and even fines content. Fig. 9b has shown that TSS20 failed in the pattern of flow-type but the TSS10 exhibited cyclic mobility, for specimens with nearly the same void ratio (e_c = 0.791 ~ 0.794) and consolidated to σ'_{nc} = 300kPa. For this reason, a more comprehensive investigation is needed to take into account the

impacts of soil states, initial static shear stress, amplitude of cyclic stress, soil properties, and so on.

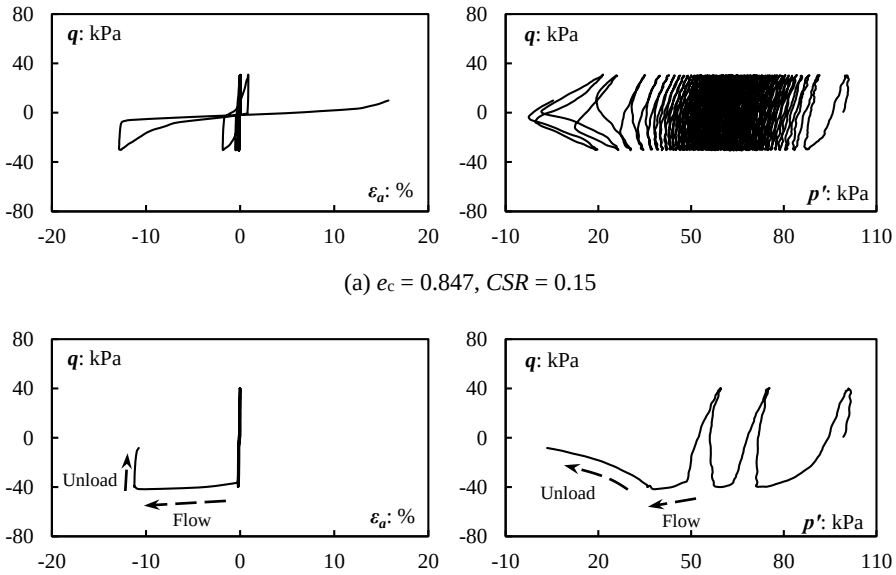

(a) e_c = 0.847, *CSR* = 0.15

(b) e_c = 0.849, *CSR* = 0.2

Fig. 8. Effect of *CSR* on failure patterns (TSS10, e_c = 0.847~0.849, α = 0, σ'_{nc} = 100kPa)

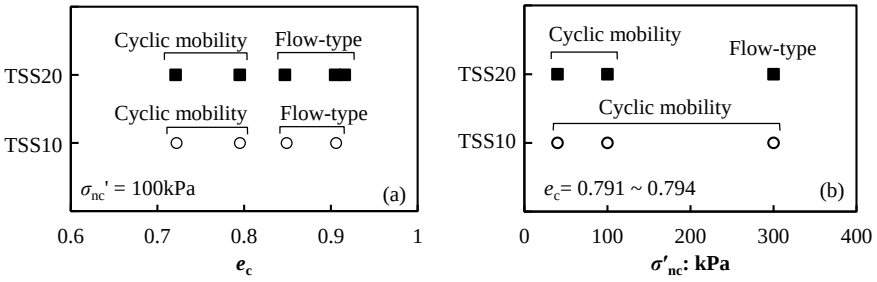

Fig. 9. Summary of effects initial states on the failure patterns of silty sands (α = 0)

5 Conclusions

In this paper, several types of cyclic failure patterns of silty sands are presented and discussed. It is found that the failure patterns turn from flow-type failure to non-flow type (i.e., cyclic mobility and plastic strain accumulation) when the packing density of the specimens increases. For loose specimens, it appears that the presence of initial static shear stress does not affect the failure pattern. However, for relatively dense specimens, the reversal condition of the cyclic loading, which is affected integrally by

the initial static shear stress and the cyclic stress amplitude, determines the failure pattern be cyclic mobility or plastic strain accumulation. In addition, the confining pressure and the amplitude of cyclic stress can also affect the failure pattern under otherwise similar conditions. The characterization of failure pattern is an important but less well-investigated issue in liquefaction evaluation, and thus, further investigations are needed.

Acknowledgement

The present study is supported by the Fundamental Research Funds for the Central Universities, Zhejiang University (2021QNA4021).

References

1. Ishihara, K.: Liquefaction and flow failure during earthquakes. Géotechnique 43(3), 351–451 (1993).
2. Castro, G.: Liquefaction and cyclic mobility of saturated sands. Journal of the Geotechnical Engineering Division 101(6), 551–569 (1975).
3. Sze, H. Y., Yang, J.: Failure modes of sand in undrained cyclic loading: impact of sample preparation. Journal of Geotechnical and Geoenvironmental Engineering 140(1), 152–169 (2014).
4. Mohamad, R., Dobry, R.: Undrained monotonic and cyclic triaxial strength of sand. Journal of Geotechnical Engineering 112(10), 941–958 (1986).
5. Chiaro, G., Koseki, J., Kiyota, T.: New insights into the failure mechanisms of liquefiable sandy sloped ground during earthquakes. In: 6th International Conference on Earthquake Geotechnical Engineering. No. 200 (2015).
6. Yang, J., Sze, H. Y.: Cyclic behaviour and resistance of saturated sand under non-symmetrical loading conditions. Géotechnique 61(1), 59–73 (2011).
7. Wichtmann, T., Kimmig, I., Steller, K., Triantafyllidis, T., Back, M., Dahmen, D.: Correlations of the liquefaction resistance of sands in spreader dumps of lignite opencast mines with CPT tip resistance and shear wave velocity. Soil Dynamics and Earthquake Engineering 124, 184–196 (2019).
8. Cubrinovski, M., Green, R., Allen, J., Ashford, S., Bowman, E., Bradley, B. A., Cox, B., Hutchinson, T., Kavazanjian, E., Orense, R.: Geotechnical reconnaissance of the 2010 Darfield (New Zealand) earthquake. Bulletin of the New Zealand Society for Earthquake Engineering 43(4), 243–320 (2010).
9. Mason, H. B., Gallant, A.P., Hutabarat, D., Montgomery, J., Reed, A. N., Wartman, J.: Geotechnical Reconnaissance: The 28 September 2018 M7.5 Palu-Donggala, Indonesia Earthquake. Geotechnical Extreme Events Reconnaissance (GEER) Association, United States (2019).
10. Wei, X., Yang, J.: Characterizing the effects of fines on the liquefaction resistance of silty sands. Soils and Foundations 59(6), 1800–1812 (2019).
11. Ladd, R.: Preparing test specimens using undercompaction. Geotechnical Test Journal 1(1), 16–23 (1978).
12. Ishihara, K.: Soil Behaviour in Earthquake Geotechnics. Oxford University Press, New York, United States (1996).